Short-Term Active Power Reduction in DFIG-Based Wind Farms for Improving First-Swing Stability in Power Systems

Yuan Liu * and Taishan Xu

Posted Date: 16 March 2026

doi: 10.20944/preprints202603.1160.v1

Keywords: DFIG; wind power; transient stability; first swing; critical clearing time (CCT)

 doi:10.20944/preprints202603.1160.v1

Article

Short-Term Active Power Reduction in DFIG-Based Wind Farms for Improving First-Swing Stability in Power Systems

Yuan Liu [1,*] and Taishan Xu [1,2]

[1] School of Electrical and Power Engineering, Hohai University, Nanjing 211100, China

[2] State Grid Electric Power Research Institute Co., Ltd. (Nanrui Group Co., Ltd.), Nanjing 211106, China

* Correspondence: yuan_liu_power@163.com

Abstract

In this paper, a short-term active power curtailment (ST-APC) strategy for doubly fed induction generator (DFIG) wind farms is proposed to enhance first-swing rotor angle stability under fault disturbances. While wind power is a clean renewable resource that is widely deployed, its large-scale integration heightens concerns about transient stability. After analysing DFIG operating principles, this study advocates for using short-horizon active power control to mitigate the adverse stability impacts of wind farms. Using the Western System Coordinating Council (WSCC) three-machine nine-bus test system, the effectiveness of the ST-APC strategy across diverse operating conditions is verified. Simulation results show that, following a fault, modulating the DFIG's active output effectively suppresses the first swing, postpones loss of synchronism, and increases the critical clearing time (CCT). The scheme yields notable benefits regarding improvements in overall stability, reductions in the frequency nadir, and acceleration of frequency recovery. Sensitivity analyses further examine the effects of activation time, control duration, and curtailment depth on CCT and offer tuning recommendations. The findings indicate that the proposed strategy is practical and adaptable, making it suitable for power systems with high wind power penetration.

Keywords: DFIG; wind power; transient stability; first swing; critical clearing time (CCT)

1. Introduction

As the global energy mix continues to shift, and nations pursue carbon neutrality (the "dual-carbon" goal), wind energy has become a major source of clean renewable electricity, and its share in power systems has increased rapidly [1]. However, the large-scale integration of wind farms has introduced unprecedented challenges for the operational stability of conventional power systems. Wind turbines are typically connected to the grid through power electronic converters, which inherently lack physical inertia and cannot buffer grid fluctuations via rotor kinetic energy like synchronous generators; thus, when severe grid disturbances occur, system frequency and rotor angles become highly sensitive—especially in hybrid operation scenarios of synchronous generators and power electronic devices—exacerbating transient stability issues. As the structure of power systems evolves, stability-related research continues to receive significant attention from the international academic community, and definitions and classifications of power system stability continue to evolve in the literature [2].

Among the various wind turbine technologies, the doubly fed induction generator (DFIG) is by far the most widely used [3]. With a rotor-side converter (RSC), DFIGs can achieve variable-speed constant-frequency operation over a broad range of wind speeds. By injecting rotor currents, they enable fast decoupled control of active and reactive power, offering excellent regulation capability and flexible power factor control [4]. With the increase in wind power penetration, the rotor angle and frequency responses of power systems grow more pronounced under large disturbances, usually

 doi:10.20944/preprints202603.1160.v1

manifested as rapid frequency drop and reduced first-swing stability [5]. The role of the fast active power control of DFIGs in supporting the frequency and angle stability is receiving increasing attention [6].

The long-term intervention mechanism of wind power affecting transient stability can be divided into steady-state effects and transient effects. Steady-state factors involve power flow redistribution and wind generator placement, whereas transient factors include system inertia, damping, and synchronising torque [7]. On the active power side, typical strategies include maximum power point tracking (MPPT) switching, adjusting the active power recovery rate (APR), or temporarily suppressing post-fault recovery to reduce the acceleration of synchronous machines [8]. On the reactive power side, voltage/reactive power support or using the grid-side converter (GSC) as a static synchronous compensator (STATCOM) can improve transient margins [9]. For virtual inertia and virtual-axis control, equivalent inertia and damping can be added to enhance first-swing performance, but these methods often require compromises among measurement noise, phase compensation, and current limits [10,11]. These studies mostly focus on long-term intervention through pre-event planning; however, in recent years, research on short-term measures for in-event emergency control after faults has also increased. During severe disturbances, the rotor angle dynamics of synchronous generators are dominated by the transient energy equation, while the system frequency response is mainly determined by the inertial response of units; however, with the increase of wind power penetration, the system equivalent inertia decreases, making it difficult to quickly respond to transient instability [12]. Doubly-fed induction generators (DFIG) have the capability of fast active power regulation, which can provide effective power support within the first swing time window after a fault, and has important application value for improving the transient stability of power systems with high wind power penetration.

In the research field of improving the transient power angle stability of power systems using short-term active power control methods, many scholars have carried out relevant explorations. Literature [13] first proposed a method to improve the transient stability of wind farms through active active power control, indicating that the output of wind farms can participate in the transient control of the system in a short time and effectively reduce the amplitude of the first swing of the power angle. However, it lacks a systematic analysis of the sensitivity of control parameters, and there is still room for optimization in the triggering logic of short-term control. Subsequently, Literature [14] further studied the influence of the active power recovery rate on the first swing stability, and reduced the system oscillation time and enhanced the short-term stability by gradually restoring the output after a fault, but still lacked an active short-term power reduction scheme and analysis of the impact of wind power access location. Literature [15] proposed a joint active-reactive power control strategy based on system frequency signals, which improves transient stability through frequency-dependent regulation and verifies the effect similar to virtual inertia, but does not optimize the design for short-term windows. Literature [16] analyzed the influence of gear ratio and reactive power control on transient stability, breaking through the traditional idea of only focusing on active output, providing a reference for optimizing parameter configuration, but did not involve the application of real-time short-term control based on local fast measurement data. Literature [17] combined uncertainty analysis with preventive control, and the proposed strategy is suitable for planning and high-level optimization stages, but still lacks a direct and feasible scheme for real-time short-term power regulation. Literature [18] used deep learning to design a fault current limiter to improve the transient stability of doubly-fed wind turbines, with significant effects, but the parameter optimization of control trigger logic, depth and duration has not been fully studied. Literature [19] proposed a virtual impedance demagnetization control strategy to enhance the transient synchronization stability of wind turbines. Most existing strategies are verified through simulations in power systems computer aided design/electromagnetic transients including direct current (PSCAD/EMTDC) and MATrix LABoratory/Simulink (MATLAB/Simulink), with evaluation indicators including rotor angle, critical clearing time (CCT), etc., which reflect the anti-disturbance capability and stability characteristics of the system. However, existing strategies still have

 doi:10.20944/preprints202603.1160.v1

shortcomings in aspects such as control accuracy, short-term window optimization, application of local rapid measurement, and trigger logic optimization. This paper proposes a short-term active power curtailment strategy based on local frequency signals, which improves scenario adaptability and control effect stability by optimizing control timing and setting adjustable curtailment amplitude and duration.

In this paper, a novel short-term active power control (ST-APC) strategy is proposed to improve the transient stability of power systems with high DFIG-based wind penetration, with particular attention to first-swing stability. The method is based on the following principle: after a fault occurs and is cleared, the rate of change in the wind farm bus frequency or rotor angle is used as a local measurement signal. Through low-pass filtering and a PI controller, a short-duration active power reduction signal is generated and superimposed on the original power reference of the DFIG. This rapid reduction decreases the post-fault electrical power input and helps the neighbouring synchronous generators decelerate more quickly without significantly affecting the long-term operation of the wind farm. It thus acts as an emergency control mechanism between inertia response and primary frequency control. Compared with traditional methods such as inertia emulation or dispatching spinning reserves, this method fully utilises the inherent flexibility of wind farms without additional hardware investment. Extensive time domain simulations under different wind-penetration levels, fault locations, and wind speed scenarios verify the robustness and applicability of the proposed control scheme.

The main contributions of this paper are summarised as follows:

1. Based on rotor angle dynamics and kinetic energy exchange principles, the influence of DFIG wind farms on first-swing stability is analysed, providing a theoretical foundation for short-term active power modulation.
2. A practical control structure based on local frequency or rotor speed estimation, including low-pass filtering and PI adjustment, is designed to realise real-time implementable ST-APC control.
3. A detailed simulation model based on the Western System Coordinating Council (WSCC) 9-bus system is developed, and by comparing key stability metrics between controlled and uncontrolled scenarios, it demonstrates the effectiveness of the proposed method in improving the CCT and suppressing angle deviations.
4. A parameter study examines the effects of control activation time, modulation duration, and depth, and wind penetration level on system stability, offering practical tuning recommendations for various operating conditions.

Through these efforts, the work extends the existing literature by promoting active power modulation of DFIGs for enhancing transient stability and offers a novel paradigm for ensuring safe operation in systems with high wind penetration.

2. Theory and Methods

2.1. Mechanism Analysis and Motivation for Short-Term Active Power Reduction

2.1.1. Power Angle Swing Equation and Equal Area Criterion

In the short time interval following a fault, the power angle dynamics are dominated by the following swing equation, as shown in Equation (1):

$$M\ddot{\delta} = P_m - P_e - P_D = \Delta P, \quad \dot{\delta} = \omega, \tag{1}$$

where M denotes the machine's electrical inertia, P_m the mechanical power, P_e the electrical power, and P_D the damping power. Because mechanical power varies only slightly within the first-swing window (usually 0.5–2 s), the transient power angle response is mainly driven by electrical power.

 doi:10.20944/preprints202603.1160.v1

According to the **equal area criterion**, as quantified by Equation (2), the energy balance of the acceleration area and deceleration area must be satisfied at the fault clearing time point to maintain system synchronism:

$$\int_{\delta_0}^{\delta_c} (P_m - P_{e2})\, d\delta = \int_{\delta_c}^{\delta_x} (P_{e1} - P_m)\, d\delta \tag{2}$$

Here, P_{e1} and P_{e2} represent the electrical power curves under different control conditions after fault clearing. $\delta_{\max}$ is the maximum first-swing angle. If P_e can be effectively increased during the fault or immediately after clearing, the acceleration area can be reduced or the deceleration area shaped to suppress the maximum first-swing angle.

Figure 1 illustrates the principle of short-term active power control: reducing the acceleration area and increasing the deceleration area by reducing the active power of a nearby wind turbine, the electromagnetic power curve of the synchronous generator is raised. When the wind farm location is electrically close to the critical synchronous generator, the effect on power angle stability can be significant.

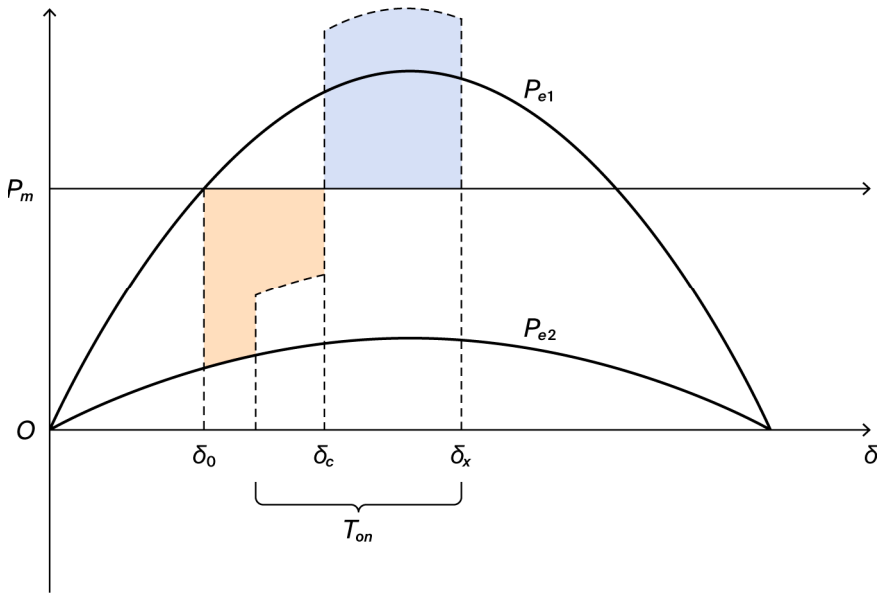

Figure 1. Principle of Wind Turbine-Assisted Transient Stability Control for Synchronous Generators. Where P_{e1}=pre-fault electromagnetic power, P_{e2}=during-fault electromagnetic power, Pm=mechanical power, δ_0=initial stable power angle, δ_c=fault clearing power angle, δ_x=power angle at the end of deceleration process, T_{on}=control action time. Before the fault, the system operates stably at the intersection δ_0 of P_{e1} and Pm; after the fault, the electromagnetic power P_e of the synchronous generator drops to P_{e2}, and the power angle swings to the right. At a certain point between δ_0 and the fault clearing power angle δ_c, the wind turbine load reduction control is activated. Due to the fixed total power demand of the system, the active power demand obtained by the synchronous generator increases, thereby raising P_e to a position higher than P_{e2} and reducing the accelerating area. At time δ_c, the fault is cleared, and because the wind turbine load reduction is still in effect, the P_e of the synchronous generator returns to a position higher than P_{e1}, increasing the decelerating area.

2.1.2. Influence Path of DFIG Active Power Modulation and the Effect of Wind Farm Location

In a two-machine–infinite-bus model, a DFIG connected to the grid can be represented as an equivalent impedance. The synchronous machine electrical power can be expressed as Equation (3):

$$P_e(\delta) = \frac{E_q^2}{|Z_{11}|}\sin\alpha_{11} - \frac{E_q V_s}{|Z_{12}|}\sin(\delta - \alpha_{12}), \tag{3}$$

 doi:10.20944/preprints202603.1160.v1

where Z_{11} and Z_{12} are the equivalent self-impedance and mutual impedance. Their relationship to the DFIG's injected active power P_w and reactive power Q_w is shown as Equation (4):

$$r_w + jX_w = -\frac{V_t^2}{P_w^2 + Q_w^2}(P_w + jQ_w). \tag{4}$$

When the wind farm active power P_w is reduced for a short period, the equivalent resistance r_w decreases, changing the magnitude and phase of Z_{11} and Z_{12}. This results in an increase in synchronous machine electrical power P_e, thereby reducing $\Delta P = P_m - P_e - P_D$ and suppressing increments in the power angle δ. The electrical coupling strength between the DFIG and synchronous machine directly affects the modulation effect: if the wind farm is connected close to the critical synchronous generator (i.e., with low intervening impedance), changes in P_w have a stronger impact. Conversely, the effect weakens if the electrical distance is large. Moreover, once the system is close to losing synchronism and the target synchronous machine is already in a "low-speed" power angle stage ($|\dot{\delta}|$ very small), even increasing P_e has limited impact. Early intervention during the fault is therefore key.

2.1.3. Analysis of Early Control Timing

From the swing equation, the energy accumulated due to power imbalance in the initial fault period determines the first-swing angle. Defining the acceleration area as Equation (5):

$$A_{\text{acc}} = \int_{\delta_0}^{\delta_c} (P_m - P_{e,\text{fault}})\, \mathrm{d}\delta, \tag{5}$$

which follows that, for the same control activation window, intervening earlier reduces the integrand and thus lowers A_{acc}. Studies have shown that activating control immediately after the fault occurs or shortly thereafter—as opposed to delaying until after clearance—produces the most significant CCT improvements. In the 9-bus system, activating control about 200 ms earlier can increase the CCT by more than 10–15 ms. Therefore, **earlier intervention is more effective**, and this temporal principle is supported by both the equal area criterion and simulation results.

2.1.4. Auxiliary Effect of Short-Term Active Power Reduction on Frequency

Assuming constant mechanical input on the generation side, reducing the active power of the DFIG decreases the total electrical power injected into the grid. The system frequency dynamics are governed by the aggregated swing equation, Equation (6).

$$\frac{2H_{\text{sys}}}{\omega_s}\dot{\omega}_{\text{COI}} = \sum_i (P_{m,i} - P_{e,i}) \;\Rightarrow\; \dot{f}_{\text{COI}} \propto \sum_i \Delta P_i, \tag{6}$$

where H_{sys} is the system inertia constant, ω_{COI} is the centre-of-inertia speed, and f_{COI} the COI frequency. By temporarily reducing the DFIG output, the electrical power of neighbouring synchronous machines P_e increases, reducing the overall ΔP and slowing the rate of frequency change. Although frequency behaviour is not the primary control variable here, moderating the frequency nadir helps lessen the burden on governor action.

2.2. Control System Structure

2.2.1. Control Objectives and Constraints

The proposed control strategy aims to enhance system transient stability during the first swing following a large disturbance. Specifically, at or immediately after the fault occurs, a short-term reduction in DFIG electromagnetic torque is commanded based on the frequency deviation measured at the wind farm bus [20]. This torque reduction signal is superimposed on the DFIG torque reference to temporarily lower the wind farm active power output, thereby increasing the electrical power

 doi:10.20944/preprints202603.1160.v1

support of adjacent synchronous generators and improving the critical clearing time. The control is active only within a short time window after the fault and then automatically withdrawn to avoid interfering with the MPPT mode. To ensure implementability, the magnitude and rate of change in the control signal must be constrained to prevent rotor current saturation or shaft torque oscillations. The framework builds on the classic "additional control block" (ACB) structure used for short-term torque modulation but moves the trigger earlier to the fault instant for more timely energy intervention.

2.2.2. Control Structure and Implementation

The control strategy uses a frequency deviation-driven adjustment to the electromagnetic torque reference [21]. An external gating block ensures that the control is only applied within a specified window. Figure 2 shows the overall control structure. The input signal is the frequency deviation at the wind farm bus, $\Delta f = \hat{f} - f_0$, where $\hat{f}$ is estimated from the derivative of the bus voltage phasor angle. A PI controller processes the frequency deviation to produce a preliminary control signal; amplitude limiting prevents excessive modulation. To improve robustness, the control signal is passed through a first-order low-pass filter to suppress high-frequency noise.

Activation of the control is governed by two conditions: (1) a fault detection module monitors voltage sag and recovery at the bus, and (2) a timer holds the control gate open for a fixed duration T_{on} seconds after activation before automatically closing. This design confines the control action to the first-swing window and avoids interfering with MPPT once stability is restored. During the active period, the final torque correction $\Delta T_e(t)$ is added to the baseline torque reference $T_{e,\text{base}}(t)$, affecting a short-term reduction in electromagnetic torque and active power output, as expressed in Equation (7).

$$\Delta P_{\text{WF}} \approx \omega_r \cdot \Delta T_e, \tag{7}$$

where ω_r is the rotor mechanical speed. Thus, by shaping ΔT_e with the PI–filter–limiter chain and gating logic, a desired temporary reduction in wind farm output is realised.

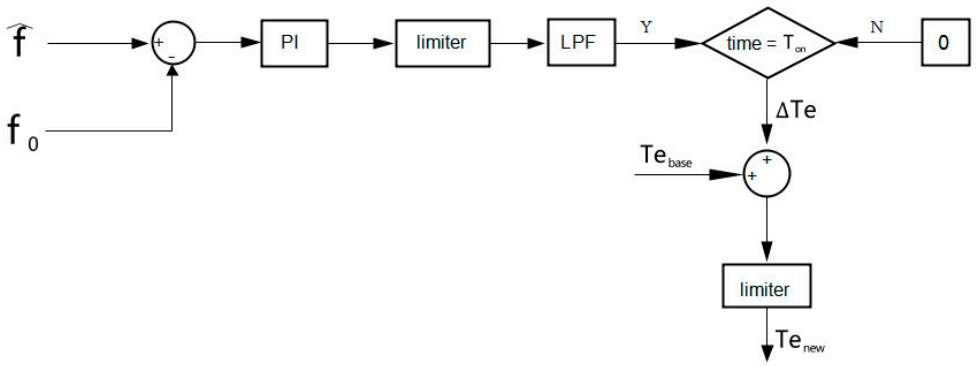

Figure 2. Control Structure of the Proposed Short-term Active Power Curtailment Strategy. Where $\hat{f}$ = estimated grid frequency, f_0 = rated grid frequency, PI = proportional-integral controller, limiter = amplitude limiter module, LPF = low-pass filter, T_{on} = control activation timer, Te_{base} = initial electromagnetic torque reference, ΔTe = torque adjustment signal, Te_{new} = updated electromagnetic torque command. Te_{base} is the original measured basic torque command of the wind turbine. When T_{on}= 1, the timing control module is activated, and ΔTe is calculated from the frequency deviation after PI regulation, amplitude limitation and low-pass filtering, and the final torque control command $Te_{new} = Te_{base} + \Delta$Te; when T_{on} = 0, the timing control module is turned off, Δ Te = 0, $Te_{new} = Te_{base}$, and the wind turbine returns to the original basic torque control.

 doi:10.20944/preprints202603.1160.v1

2.3. Simulation Setup

2.3.1. Simulation Platform and System Model

Simulations were performed in the OpenModelica 1.25.4 environment (https://openmodelica.org) using the OpenIPSL 3.1.0 library. The test system is the WSCC 3-machine 9-bus system. A wind farm modelled on a GE Type-3 DFIG is aggregated and connected to the load bus through a transformer, as shown in Figure 3.

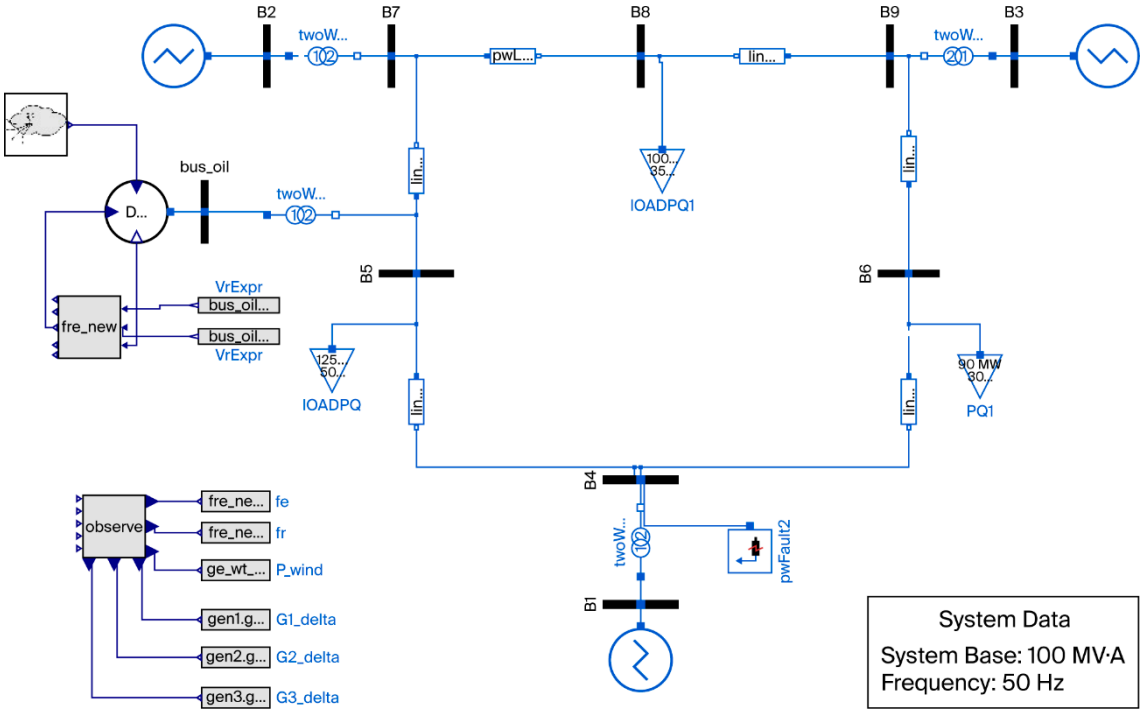

Figure 3. Connection of the wind farm to the WSCC 9-bus system.

Figure 4a depicts the internal modification of the GE Type-3 model. The DFIG model consists of a turbine, electrical_control, and generator sub-modules; the power-order variable, pord, is the output of the turbine module and an input to the electrical_control module. To introduce the control, this link is broken: the pord port of the turbine feeds into the frequency-power controller, and the adjusted pord value is input to electrical_control. This variable represents the active power reference of the wind turbine, and adjusting it effectively modifies the electromagnetic torque reference of the rotor side converter and thus the wind turbine output.

Figure 4b shows the external wiring of the frequency-power controller. In addition to the pord signal, the controller receives the v_r and v_i variables from the bus to which the turbine is connected. These represent the real and imaginary parts of the bus voltage phasor and are used to calculate the frequency deviation.

Figure 4c illustrates the internal structure of the controller. Frequency deviation is estimated using Equation (8).

$$\Delta\omega = \frac{v_r\dot{v}_i - v_i\dot{v}_r}{v_r^2 + v_i^2}, \qquad \Delta f = \frac{\Delta\omega}{2\pi}, \tag{8}$$

where in the phasor model of OpenModelica/OpenIPSL the v_r and v_i variables represent the positive-sequence voltage components with the 50 Hz base frequency removed. Therefore, the resulting $\Delta\omega$ is a **frequency deviation** rather than the absolute frequency. To obtain the actual frequency, the rated frequency (50 Hz) must be added: $f = 50 + \Delta\omega/(2\pi)$. After computing, Δf of the signal passes through a PI controller, limiter, and low-pass filter to generate the control signal; a

 doi:10.20944/preprints202603.1160.v1

Boolean table and switch module implement the timing mechanism that selects whether the pord remains unchanged or is regulated.

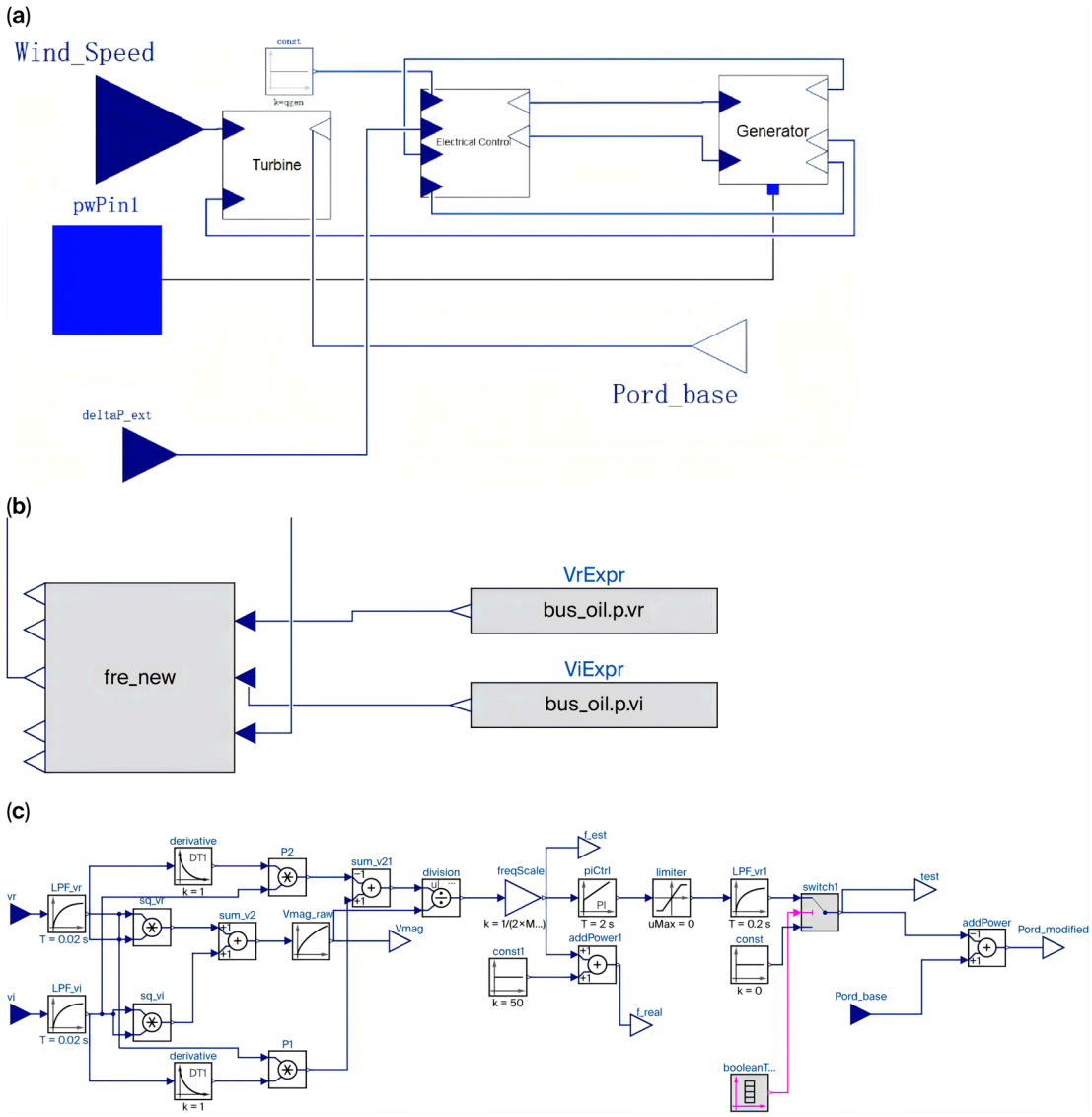

Figure 4. (**a**) Modified internal structure of the GE Type-3 model. (**b**) External wiring of the frequency-power controller. (**c**) Internal structure of the frequency-power controller.

2.3.2. Simulation Scenarios and Measured Variables

The baseline wind speed is 14 m/s, and the wind farm steady-state output is approximately 50 MW. The initial values of the wind generator, synchronous generators, and loads are summarised in Table 1. The relevant DFIG parameters are listed in Table 2.

Table 1. Initial conditions of selected devices.

Equipment Type	Device Name	Bus	P_0 (MW)	Q_0 (MVAr)	V_0	Angle_0 (deg)
Wind generator (DFIG)	GE_WT	Bus_oi1	50	5	1.000	0
Synchronous generator	Gen1	B2	163	6.65	1.025	9.28
Synchronous generator	Gen2	B3	85	−10.86	1.025	4.66
Synchronous generator	Gen3	B1	71.64	27.05	1.040	0
Load	10ADPQ	B5	125	50	0.995	−3.99
Load	PQ1	B6	90	30	1.013	−3.687
Load	10ADPQ	B8	100	35	1.016	0.728

 doi:10.20944/preprints202603.1160.v1

Table 2. Parameters related to wind turbines.

Parameter	GEN_base (MVA)	WT_base (MVA)	Freq (Hz)	Poles	$p_{w,max}$	$p_{w,min}$	K_{Oi}	K_{Vi}
Value	100	100	50	3	1.12	0.1	0.3	5
Parameter	x_{iqmax}	x_{iqmin}	n_{mass}	H_g (s)	H (s)	K_{tg}	D_{tg}	K_l
Value	1	−1	2	0.62	4.33	1.11	1.5	56.6

Two sets of simulations are designed to evaluate the control strategy:

- **Baseline case (no control):** The DFIG operates under maximum power point tracking (MPPT) with no additional control logic. Both fault and no-fault conditions are considered.
- **Controlled case (short-term active power reduction):** A three-phase short-circuit fault is applied at the load bus. The gating logic is triggered based on the voltage sag and preset timing. When triggered, the controller reduces `pord` by 0.6 pu for 3 s; the control signal is limited and low-pass filtered before injection.

Parameter sensitivity studies vary the control initiation time, control duration, control depth, wind farm location, and system power flow relative to the controlled case.

The following indicators are monitored: (1) wind farm output power—recording the change in pord and $P_{WF}(t)$; (2) system frequency response—tracking the minimum frequency f_{min} and recovery time t_{rec} (defined as the first time the frequency returns to within ±0.05 Hz); (3) synchronous generator rotor angle dynamics—monitoring the relative rotor angle δ_{21} and extracting the maximum first-swing deviation δ_{max}; (4) critical clearing time (CCT)—determined via a bisection search for the fault clearing limit, using generator desynchronism or unrecovered frequency as the criterion. All simulations use the DASSL solver with an adaptive time step (relative tolerance set to 1e−6) and cover a 0–10 s window to include fault occurrence, clearing, and short-term recovery.

3. Results

3.1. Uncontrolled Case

Without faults, the variables pord, P_{WF}, frequency f and rotor angle δ evolve as shown in Figure 5. The pord reference reaches a steady value of 1.12 pu at about 2.8 s. Wind farm power P_{WF} initially rises in conjunction with pord to a peak before gradually declining; with a longer simulation window, it would settle at around 58 MW. Frequency gradually increases. Taking the rotor angle of Gen1 as the reference, the relative angles of Gen2 and Gen3 remain below π, indicating stable power angle behaviour.

When a three-phase fault is applied at bus B4 at $t = 3$ s with $R = 0.001$ pu and $X = 0$, the fault duration is increased in 0.01 s increments. It is found that, with a duration $T_{on} = 0.45$ s, the synchronous machine rotor angles remain stable, whereas at $T_{on} = 0.46$ s they lose synchronism (Figure 6).

3.2. Controlled Case (ST-APC)

For the controlled case, the fault duration is set to 0.4 s. At $t = 3$ s a fault occurs and the voltages at the faulted bus (bus 4) and wind farm bus (bus 5) drop (Figure 7a). If the control is activated immediately, pord is reduced by 0.6 pu for 3 s and returns to the MPPT trajectory when the control gate closes (Figure 7b). Figure 7c compares the wind farm active power with and without the control. Due to the fault-induced transients, power oscillations increase, and during the control, the power is significantly lower. Figure 7d shows that the system frequency nadir is notably reduced by the control. When testing the CCT, convergence is observed at a fault duration of 0.50 s and divergence at 0.51 s; thus, the critical clearing time is raised to 0.50 s (Figure 8).

 doi:10.20944/preprints202603.1160.v1

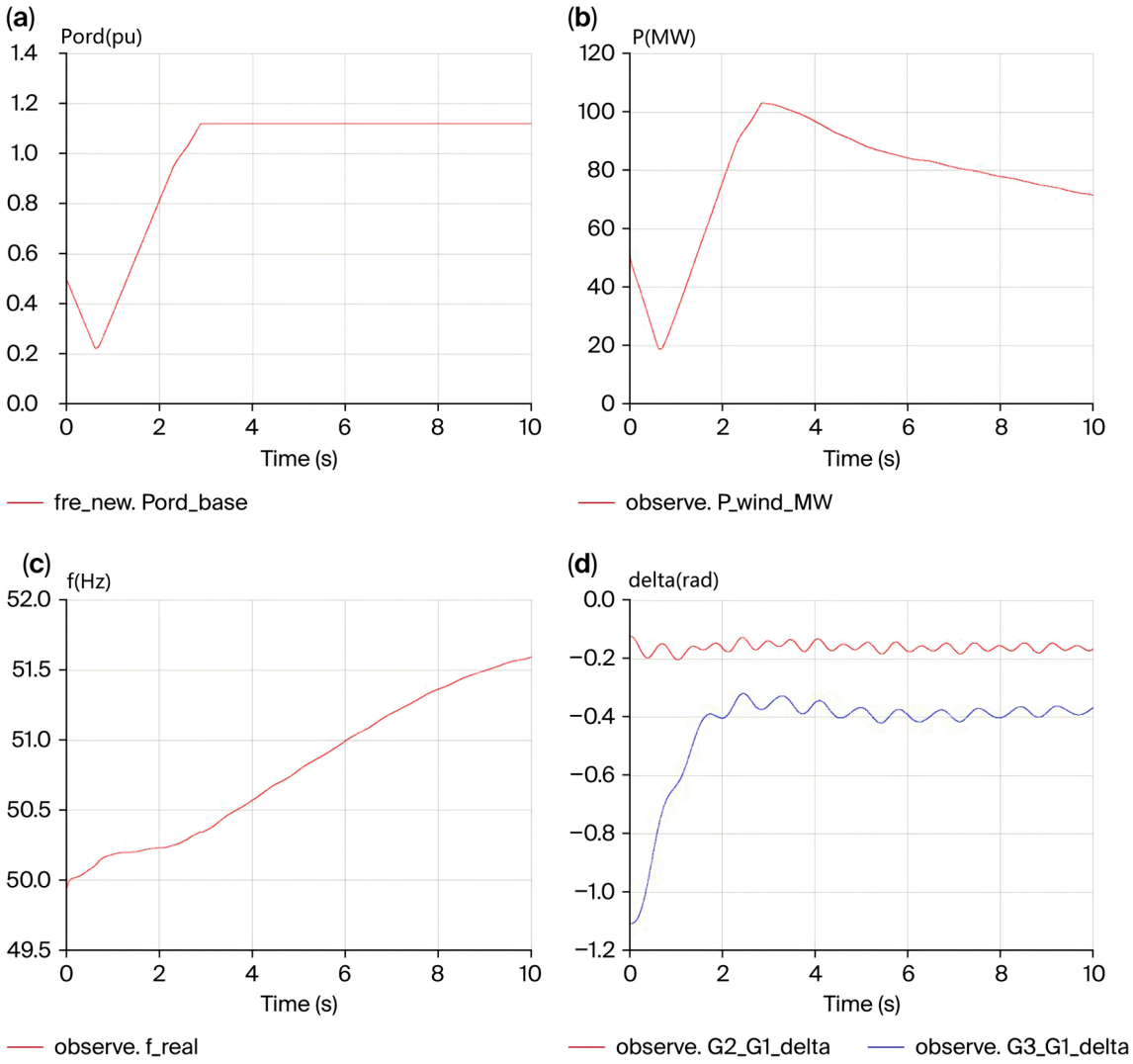

Figure 5. System response without fault: (**a**) power control variable (pord) profile; (**b**) wind farm active power P_{WF}; (**c**) system frequency f; (**d**) relative rotor angles of Gen2 and Gen3 with respect to Gen1.

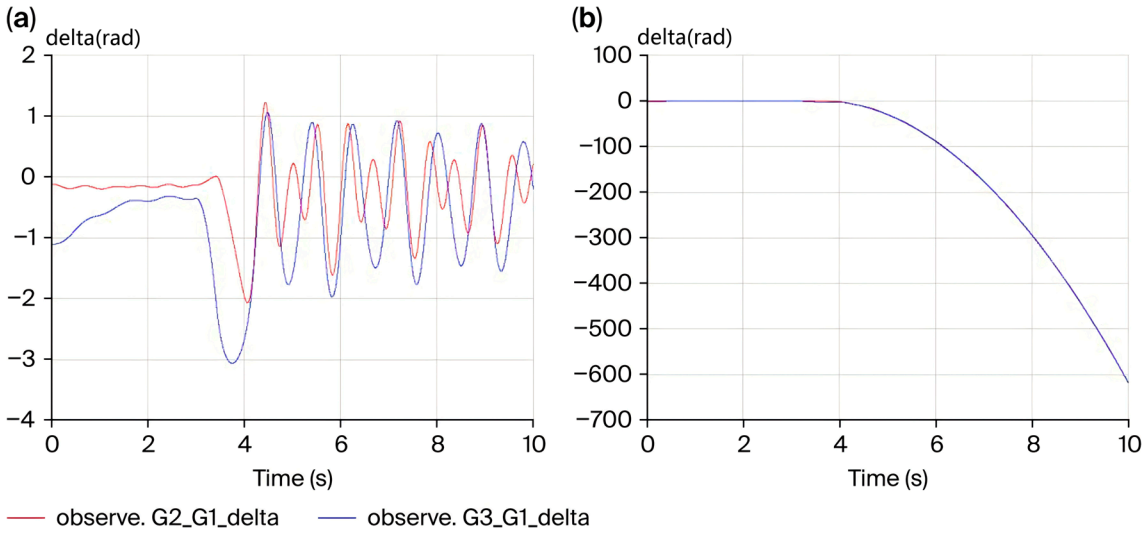

Figure 6. Rotor angle stability under different fault durations: (**a**) $T_{on} = 0.45$ s; (**b**) $T_{on} = 0.46$ s.

During the control, wind farm output declines and synchronous generator electrical power rises, resulting in a lower frequency nadir and faster recovery in the first swing. Rotor angle deviations converge, and the CCT is significantly higher than in the baseline case.

 doi:10.20944/preprints202603.1160.v1

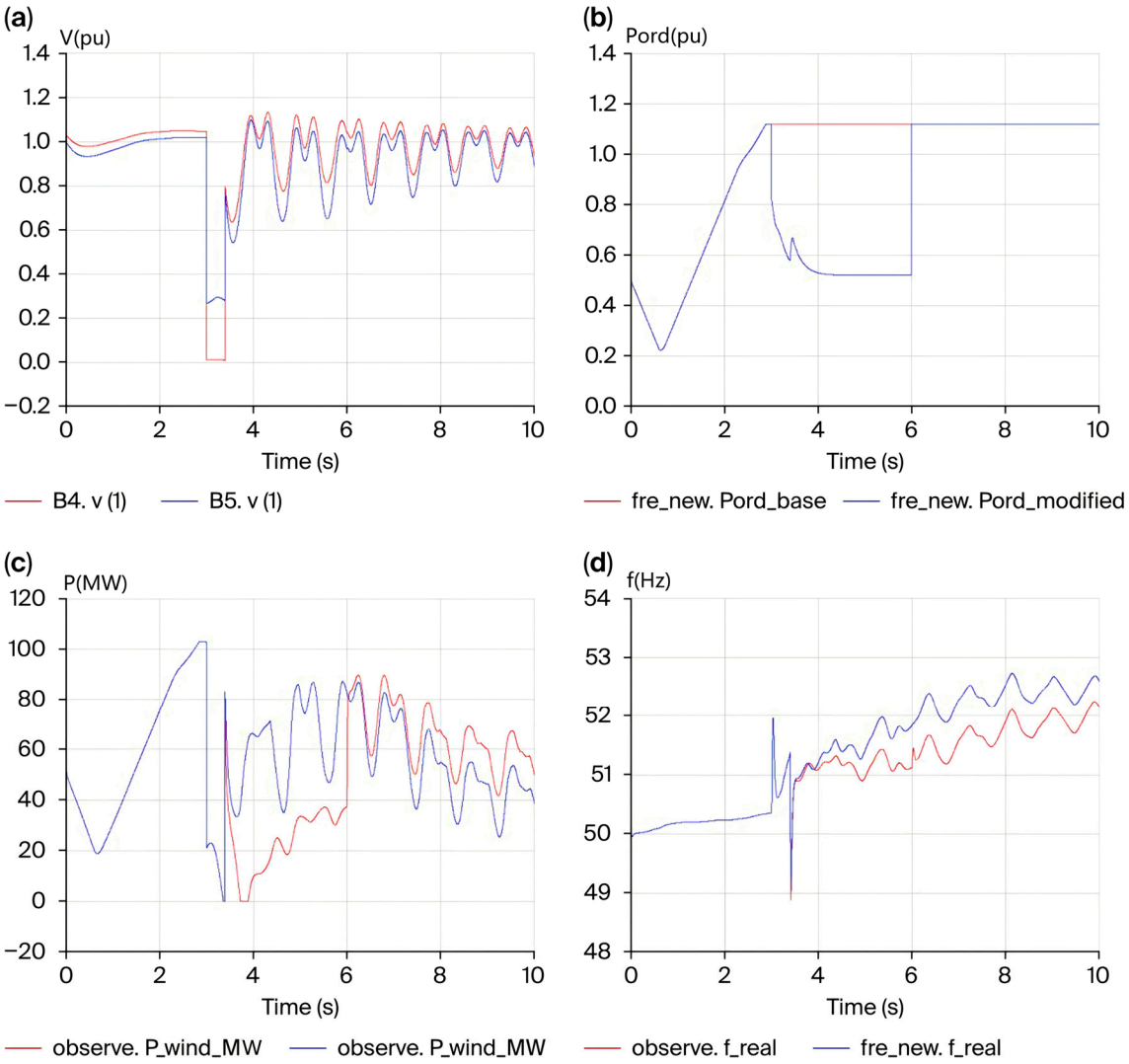

Figure 7. Comparisons of key parameters before and after implementing frequency-power control: (**a**) Voltages at B4 and B5. (**b**) Original and adjusted values of pord. (**c**) Comparison of the wind turbine active power before and after control. (**d**) Comparison of system frequency before and after control.

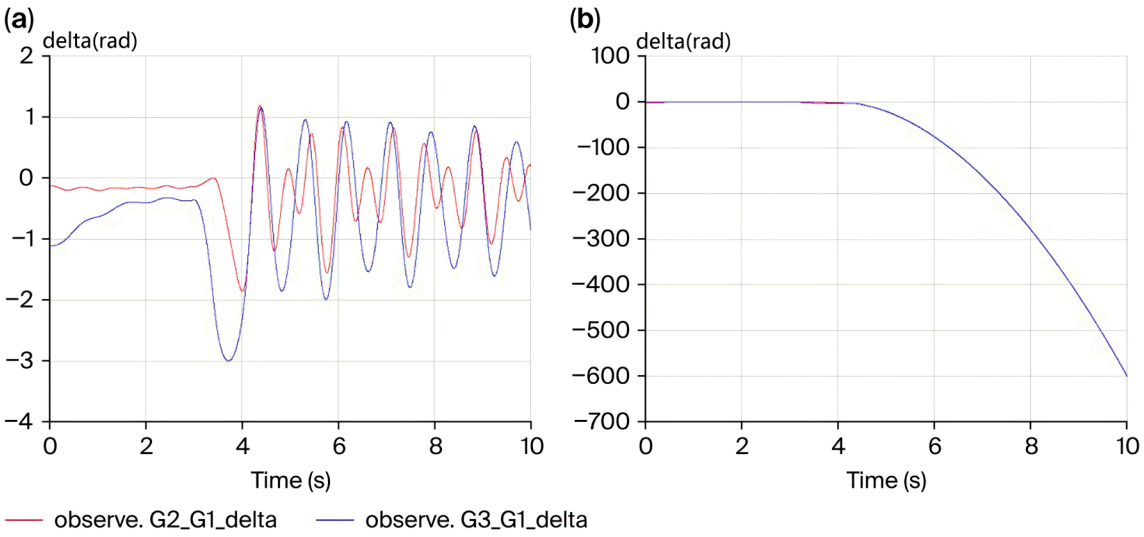

Figure 8. Critical clearing time under controlled conditions: (**a**) Power angle when fault duration is 0.49 s. (**b**) Power angle when fault duration is 0.50 s.

 doi:10.20944/preprints202603.1160.v1

3.3. Parameter Sensitivity Analysis

To assess the influence of the control parameters on system response, the control initiation time, control duration, control depth, wind farm location, and system power flow were varied. The results are as follows:

1. **Control initiation time:** The earlier the control starts, the greater the improvement in CCT. As shown in Table 3 (control depth $\Delta\text{pord} = -0.6$, wind farm at bus B7, duration fixed at 3 s), delaying the control weakens its effectiveness. In particular, control within 0.2 s of the fault yields a notable CCT improvement.
2. **Control duration:** As seen in Table 4 ($\Delta\text{pord} = -0.6$, wind farm at bus B7, initiation at the fault time), a duration around 0.5 s is optimal. The duration exhibits a characteristic "U-shaped" optimum region—in the 9-bus system, it is about 0.7–1.0 s.
3. **Control depth:** As indicated in Table 5 (duration 3 s, wind farm at bus B7), deeper control generally enhances CCT, but excessive depth may induce secondary oscillations or increase mechanical stress on the turbine.
4. **Wind farm location:** The effect varies with bus location. Table 6 shows that when $\Delta\text{pord} = -0.6$ and duration 3 s, the CCT improvement differs among buses; proximity to the critical synchronous machine is advantageous.
5. **System power flow:** The base power flow pattern also matters. If the wind farm is connected near a synchronous generator with slow rotor angle dynamics, reducing the wind farm power increases the deceleration area of adjacent generators but has little effect on remote generators that are prone to divergence. Table 7 compares a base case with 125 MW load at bus B5 and a high-load case (175 MW). The improvement is more pronounced in the base case.

Table 3. Influence of control initiation time on CCT (Δpord = −0.6, B7, duration = 3 s).

Control window (s)	[3, 6]	[3.2, 6.2]	[3.4, 6.4]	[3.6, 6.6]	[3.8, 6.8]	[4.0, 7.0]
CCT (s)	0.51	0.47	0.46	0.46	0.46	0.46

Table 4. Influence of control duration on CCT (Δpord = −0.6, B7).

Control duration	0.1 s	0.5 s	1 s	2 s	3 s
CCT (s)	0.48	0.51	0.50	0.50	0.50

Table 5. Influence of control depth on CCT (duration = 3 s, B7).

Δpord	Uncontrolled	−0.2	−0.3	−0.4	−0.5	−0.6	−0.7
CCT (s)	0.45	0.46	0.46	0.47	0.49	0.51	0.53

Table 6. Influence of wind farm location on CCT improvement (Δpord = −0.6, duration = 3 s).

Wind farm Bus	CCT Without Control (s)	CCT with Control (s)	ΔCCT (s)
B5	0.45	0.50	0.05
B7	0.46	0.51	0.05
B8	0.42	0.46	0.04

Table 7. CCT improvement under different system power flows.

Load at B5	Wind farm Bus	Control Strategy	CCT (s)	ΔCCT (s)
125 MW	B5	None	0.45	0.05
		[3 s, 6 s], −0.6 pu	0.50	
	B7	None	0.46	0.05
		[3 s, 6 s], −0.6 pu	0.51	
175 MW	B5	None	0.41	0
		[3 s, 6 s], −0.6 pu	0.41	

 doi:10.20944/preprints202603.1160.v1

	B7	None	0.37	0.04
		[3 s, 6 s], −0.6 pu	0.41	

3.4. Summary

The simulation results demonstrate that the proposed short-term active power reduction control effectively improves the frequency and rotor angle responses under fault disturbances and increases the critical clearing time. The control window and depth have a significant impact on effectiveness. The modelling framework in OpenModelica is readily reproducible and provides a foundation for extending to multi-bus, multi-wind scenarios.

4. Discussions

In this paper, a DFIG-based short-term active power control strategy driven by frequency deviation feedback is proposed to enhance first-swing stability in power systems. The control acts within a time window immediately after a fault is cleared, reducing the active output of the wind farm and thereby increasing the electrical power support of neighbouring synchronous generators. The resulting reduction in frequency nadir and power angle deviation increases the critical clearing time (CCT). Control signals are generated by processing the local frequency deviation through a PI controller with amplitude limiting, low-pass filtering, and gating logic, and are injected into the electromagnetic torque reference of the rotor side converter.

Comparative simulations on the WSCC 9-bus system show that the method improves system stability under various conditions. Typical cases achieve a CCT increase of 10–20 ms, with reduced frequency nadir and shorter recovery time.

Further analysis reveals that the performance of the control strategy depends strongly on the triggering time, control depth (ΔP), and duration (T_{on}). Triggering too early (before voltage recovery) or too late (after the first swing is formed) reduces the benefit. A combined "voltage recovery + frequency or ROCOF threshold" trigger without crowbar activation is more reliable, balancing responsiveness and practicality. The magnitude and duration of the control also exhibit a nonlinear optimum region, producing a U-shaped response surface. For example, the present study uses $\Delta P = 0.6$ pu and $T_{\text{on}} = 3$ s as a "deep–short" baseline, and parameter scanning suggests an optimal window of roughly 0.7–1.0 s. Additionally, wind speed variations and ramping can affect the initial operating point and inertia characteristics, influencing control effectiveness. In extreme cases (e.g., high wind speed ramp-up), even the polarity of the PI controller may need adjustment to avoid phase lag, causing reverse effects.

5. Conclusions

In summary, the proposed short-term active power reduction strategy significantly enhances first-swing stability without altering the basic structure or long-term operation of the DFIG. It relies only on local frequency estimation and gating signals, making it easy to integrate into existing wind farm control systems. Its main advantages include the following:

1. **Simplicity and tunability:** The control has a simple structure with easily adjustable parameters and is compatible with standard DFIG control interfaces.
2. **Transient-only action:** The control operates only during the first-swing window and does not interfere with subsequent steady-state operation.
3. **Non-intrusive integration:** The controller can be connected to the wind turbine control system without invasive modifications, facilitating deployment and scaling.
4. **Robustness across scenarios:** The strategy performs well under different connection points, wind penetration levels, and wind speed scenarios.

Future research directions include (1) coordinated control between this strategy and reactive power/voltage support from the GSC; (2) extending the logic to Type-4 (full converter) wind turbines; (3) using phasor measurement unit (PMU) angle differences and ROCOF as hybrid measurements to

 doi:10.20944/preprints202603.1160.v1

optimise triggering; (4) developing multi-machine coordinated control frameworks for large systems (e.g., IEEE 39/118-bus networks); and (5) embedding the control into dispatch systems to combine wind farm active power scheduling with transient stability control.

Supplementary Materials: The following supporting information can be downloaded at the website of this paper posted on Preprints.org.

Author Contributions: Conceptualization, Yuan Liu and Taishan Xu; methodology, Yuan Liu; modeling, Yuan Liu; validation, Yuan Liu and Taishan Xu; formal analysis, Yuan Liu; investigation, Yuan Liu; resources, Taishan Xu; data curation, Yuan Liu; writing-original draft preparation, Yuan Liu; writing-review and editing, Yuan Liu and Taishan Xu; visualization, Yuan Liu; supervision, Taishan Xu; project administration, Taishan Xu. All authors have read and agreed to the published version of the manuscript.

Funding: This research received no external funding. The APC was funded by Yuan Liu.

Data Availability Statement: The raw/processed data required to reproduce these findings cannot be shared at this time due to the complexity of data sharing.

Conflicts of Interest: The authors declare no conflict of interest.

References

1. Kundur, P.; Paserba, J.; Ajjarapu, V.; Andersson, G.; Bose, A.; Canizares, C.; Hatziargyriou, N.; Hill, D.; Stankovic, A.; Taylor, C.; Van Cutsem, T.; Vittal, V. Definition and Classification of Power System Stability. IEEE Trans. Power Syst. 2004, 19 (3), 1387–1401. https://doi.org/10.1109/TPWRS.2004.825981.
2. Hatziargyriou, N.; Milanovic, J.; Rahmann, C.; Ajjarapu, V.; Canizares, C.; Erlich, I.; Hill, D.; Hiskens, I.; Kamwa, I.; Pal, B.; Pourbeik, P.; Sanchez-Gasca, J.; Stankovic, A.; Van Cutsem, T.; Vittal, V.; Vournas, C. Definition and Classification of Power System Stability—Revisited & Extended. IEEE Trans. Power Syst. 2021, 36 (4), 3271–3281. https://doi.org/10.1109/TPWRS.2020.3041774.
3. Gautam, D.; Vittal, V.; Harbour, T. Impact of Increased Penetration of DFIG-Based Wind Turbine Generators on Transient and Small Signal Stability of Power Systems. IEEE Trans. Power Syst. 2009, 24 (3), 1426–1434. https://doi.org/10.1109/TPWRS.2009.2021234.
4. Ekanayake, J. B.; Holdsworth, L.; Wu, X. G.; Jenkins, N. Dynamic Modeling of Doubly Fed Induction Generator Wind Turbines. IEEE Trans. Power Syst. 2003, 18 (2), 803–809. https://doi.org/10.1109/TPWRS.2003.811178.
5. Vittal, E.; O'Malley, M.; Keane, A. Rotor Angle Stability with High Penetrations of Wind Generation. IEEE Trans. Power Syst. 2012, 27 (1), 353–362. https://doi.org/10.1109/TPWRS.2011.2161097.
6. Hughes, F. M.; Anaya-Lara, O.; Jenkins, N.; Strbac, G. Control of DFIG-Based Wind Generation for Power Network Support. IEEE Trans. Power Syst. 2005, 20 (4), 1958–1966. https://doi.org/10.1109/TPWRS.2005.857275.
7. Yuan, J.; Ma, M.; Jia, Y. Transient Stability Analysis for the Wind Power Grid-Connected System: A Manifold Topology Perspective on the Global Stability Domain. Electricity 2025, 6 (3), 44. https://doi.org/10.3390/electricity6030044.
8. Gu, Y.; Zhou, Y. Analysis on the Influence of the Active Power Recovery Rate on the Transient Stability Margin of a New Power System. Processes 2025, 13 (7), 2020. https://doi.org/10.3390/pr13072020.
9. Ullah, N. R.; Thiringer, T.; Karlsson, D. Temporary Primary Frequency Control Support by Variable Speed Wind Turbines—Potential and Applications. IEEE Trans. Power Syst. 2008, 23 (2), 601–612. https://doi.org/10.1109/TPWRS.2008.920076.
10. Pradhan, C.; Bhende, C. N.; Samanta, A. K. Adaptive Virtual Inertia-Based Frequency Regulation in Wind Power Systems. Renew. Energy 2018, 115, 558–574. https://doi.org/10.1016/j.renene.2017.08.065.
11. Hu, J.; Chi, Y.; Tian, X.; Li, Y.; Xiao, Y.; Cheng, F. A Survey on Development and Prospect of Wind Turbines Virtual Synchronous Control Technology. Energy Rep. 2022, 8 (Suppl. 1), 75–83. https://doi.org/10.1016/j.egyr.2021.11.005.

 doi:10.20944/preprints202603.1160.v1

12. Ngamroo, I. Review of DFIG Wind Turbine Impact on Power System Dynamic Performances. IEEJ Trans. Electr. Electron. Eng. 2017, 12 (3), 301–311. https://doi.org/10.1002/tee.22379.
13. Mitra, A.; Chatterjee, D. Active Power Control of DFIG-Based Wind Farm for Improvement of Transient Stability of Power Systems. IEEE Trans. Power Syst. 2016, 31 (1), 82–93. https://doi.org/10.1109/TPWRS.2015.2397974.
14. Munkhchuluun, E.; Meegahapola, L.; Vahidnia, A. Impact of Active Power Recovery Rate of DFIG Wind Farms on First Swing Rotor Angle Stability. IET Gener. Transm. Distrib. 2020, 14 (25), 6041–6048. https://doi.org/10.1049/iet-gtd.2020.1072.
15. Yagami, M.; Ichinohe, M.; Tamura, J. Enhancement of Power System Transient Stability by Active and Reactive Power Control of Variable Speed Wind Generators. Appl. Sci. 2020, 10 (24), 8874. https://doi.org/10.3390/app10248874.
16. Shabani, H. R.; Hajizadeh, A.; Kalantar, M.; Lashgari, M.; Nozarian, M. Transient Stability Analysis of DFIG-Based Wind Farm-Integrated Power System Considering Gearbox Ratio and Reactive Power Control. Electr. Eng. 2023, 105, 3719–3735. https://doi.org/10.1007/s00202-023-01906-3.
17. Bian, Y.; Wan, X.; Zhou, X. Transient Stability Preventive Control of Wind Farm Connected Power System Considering the Uncertainty. Energy Eng. 2024, 121 (6), 1637–1656. https://doi.org/10.32604/ee.2024.047678.
18. Wang, Y. Enhancing Transient Stability of DFIG-Based Wind Turbine Systems Using Deep Learning-Controlled Resistance-Based Fault Current Limiters. Adv. Eng. Intell. Syst. 2024, 3 (1), e423904. https://doi.org/10.22034/aeis.2024.423904.1139.
19. Wang, X.; Chang, X.; Yan, M.; Huang, Z.; Wu, C. Transient Synchronization Stability Analysis of DFIG-Based Wind Turbines with Virtual Resistance Demagnetization Control. Electronics 2026, 15 (2), 467. https://doi.org/10.3390/electronics15020467.
20. Gupta, A. K.; Verma, K. S.; Niazi, K. R. Dynamic Impact Analysis of DFIG-Based Wind Turbine Generators on Low-Frequency Oscillations in Power System. IET Gener. Transm. Distrib. 2017, 11 (18), 4500–4510. https://doi.org/10.1049/iet-gtd.2017.0308.
21. Mariprasath, T.; Kirubakaran, V. A Critical Review on the Characteristics of Alternating Liquid Dielectrics and Feasibility Study on Pongamia Pinnata Oil as Liquid Dielectrics. Renew. Sustain. Energy Rev. 2016, 65, 784–799. https://doi.org/10.1016/j.rser.2016.07.036.